ADVANCED FUNCTIONAL MATERIALS
www.afm-journal.de

Highly Connected Silicon–Copper Alloy Mixture Nanotubes as High-Rate and Durable Anode Materials for Lithium-Ion Batteries

Hucheng Song, Hong Xiang Wang, Zixia Lin, Xiaofan Jiang, Linwei Yu, Jun Xu,* Zhongwei Yu, Xiaowei Zhang, Yijie Liu, Ping He, Lijia Pan, Yi Shi, Haoshen Zhou, and Kunji Chen*

Seeking high-capacity, high-rate, and durable anode materials for lithium-ion batteries (LIBs) has been a crucial aspect to promote the use of electric vehicles and other portable electronics. Here, a novel alloy-forming approach to convert amorphous Si (a-Si)-coated copper oxide (CuO) core–shell nanowires (NWs) into hollow and highly interconnected Si–Cu alloy (mixture) nanotubes is reported. Upon a simple H_2 annealing, the CuO cores are reduced and diffused out to alloy with the a-Si shell, producing highly interconnected hollow Si–Cu alloy nanotubes, which can serve as high-capacity and self-conductive anode structures with robust mechanical support. A high specific capacity of 1010 mAh g^{-1} (or 780 mAh g^{-1}) has been achieved after 1000 cycles at 3.4 A g^{-1} (or 20 A g^{-1}), with a capacity retention rate of ≈84% (≈88%), without the use of any binder or conductive agent. Remarkably, they can survive an extremely fast charging rate at 70 A g^{-1} for 35 runs (corresponding to one full cycle in 30 s) and recover 88% capacity. This novel alloy-nanotube structure could represent an ideal candidate to fulfill the true potential of Si-loaded LIB applications.

1. Introduction

High-rate performance and long-term stability are crucial aspects to promote the application of high-capacity silicon-loaded lithium-ion batteries (LIBs). Silicon (Si) has been well known as an outstanding candidate for LIBs, with a high lithium storage capacity of 4200 mAh g^{-1} and a relatively low lithium insertion potential.[1–3] However, the process of lithium-ion (Li-ion) insertion comes with a huge volume change as large as 400% that will cause a radical pulverization/fracture in the Si host and rapid capacity fading.[4,5] A common strategy to address this issue is to explore various nanostructured Si materials, including Si nanoparticles (NPs), Si nanowires (NWs), and nanotubes, which can help to accommodate the large volumetric change during charge/discharge cycling.[6–9]

Among them, NW core–shell structures have attracted particular interests, where the NW core can be optimized to serve as efficient electric pathway, while the outer sidewall-coated Si thin film shell has a large interface for fast Li-ion interaction or insertion. For example, a *homogeneous* core–shell structure with amorphous Si (a-Si) shell coated upon c-Si NW cores has demonstrated an improved stability compared to that with only c-Si NWs core via a suitable voltage control.[10] Replacing c-Si NW core with more stable and conductive carbon nanofibers, in a *heterogeneous* core–shell configuration, promotes both the rate performance and the stability of the LIBs.[11] Recently, H. Wu et al. proposed a hollow double-walled Si nanotube which was fabricated in a two-step synthesis, where an a-Si coating (of ≈30 nm) layer was first deposited upon a 3D polymer fiber network and then the polymer fiber cores are removed by heating in air at 500 °C to leave a hollow a-Si nanotube.[12] The advantage of such a hollow nanotube structure is obvious because the huge volume expansion of the a-Si shell (surrounded by an ion-permeable silicon oxide shell) can be easily relaxed *inward* instead of expanding *outward* (that could otherwise break the outer protective oxide shell). This has led to an excellent stability that survives 6000 runs at 12 C charge/discharge rate while maintaining a specific capacity ≈600 mAh g^{-1}. However, as the a-Si shell is poorly conductive, the thickness of the a-Si storage medium shell has to be thin enough (usually below ≈30 nm[12] to facilitate Li-ion insertion or extraction, which thus seriously limits the effective Si loading of LIBs.

H. Song, H. X. Wang, Dr. Z. Lin, X. Jiang, Prof. L. Yu, Prof. J. Xu, Z. Yu, X. Zhang, Prof. L. Pan, Prof. Y. Shi, Prof. K. Chen
National Laboratory of Solid State Microstructures and School of Electronics Science and Engineering/Collaborative Innovation Center of Advanced Microstructures
Nanjing University
Nanjing 210093, P. R. China
E-mail: yulinwei@nju.edu.cn; linwei.yu@polytechnique.edu; junxu@nju.edu.cn
Dr. Y. Liu, Prof. P. He, Prof. H. Zhou
College of Engineering and Applied Sciences
Nanjing University
Nanjing 210093, P. R. China

DOI: 10.1002/adfm.201504014

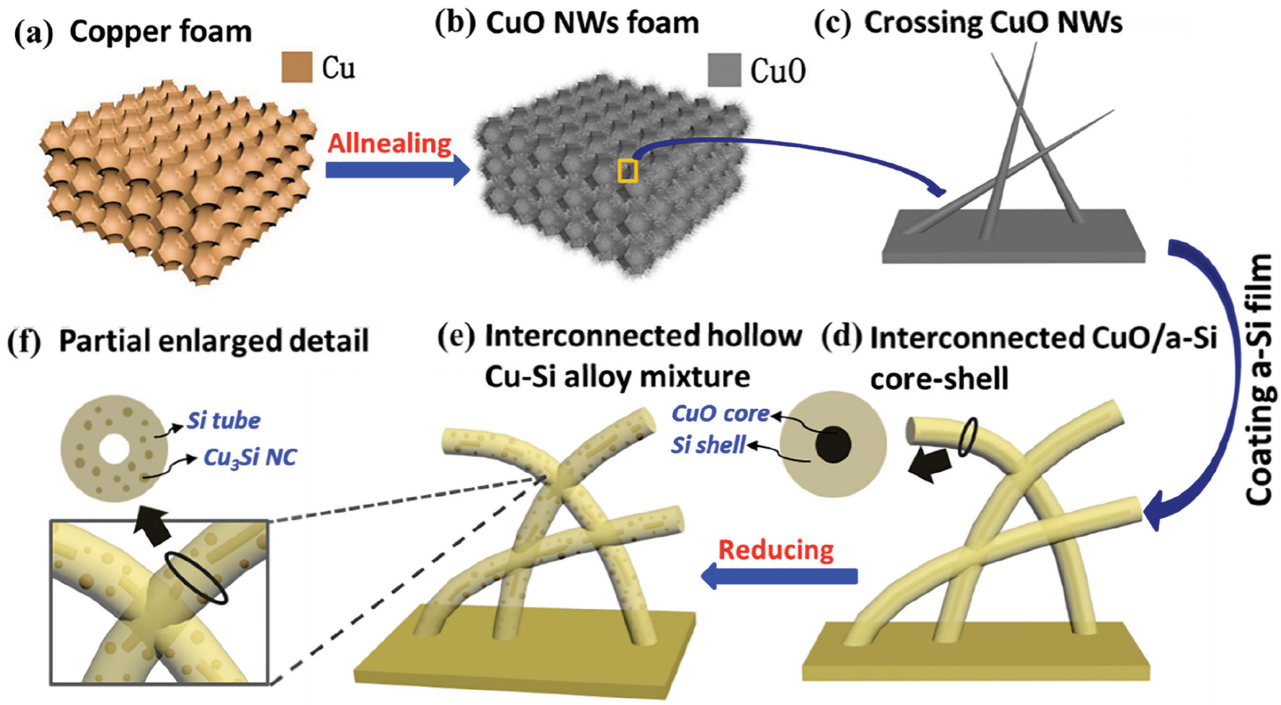

Figure 1. Schematic diagrams illustrate the synthesis process of the connected Cu–Si alloy-nanotube structures: a) copper foam substrate, b) CuO NWs grown on copper foam, c) crossing CuO NWs after thermal oxidation growth in atmosphere, d) interconnected CuO/a-Si core–shell after a-Si thin film coating, and e) the final interconnected Cu–Si nanotube anodes.

On the other hand, in pursuit of a better cycling stability, interconnected nanostructures forming multiple conductive pathways down to the collector, as schematically depicted in **Figure 1**, are indeed advantageous in maintaining a robust mechanical support and electric contact to the underlying collector. For example, Nguyen et al. have reported a highly interconnected bending Si NWs structure as anode material to improve the stability of LIB with a nearly 100% charge retention after 40 cycles at C/2 (2.1 A g^{-1}) rate and ≈1800 mAh g^{-1} after 70 cycles at 2 C (8.4 A g^{-1}).[13] Zhang et al. synthesized interconnected porous Si/C composites to show a high specific capacity and long cycle life (≈800 mAh g^{-1} after 100 cycles at 50 mA g^{-1}, an average capacity fading rate of 0.15% per cycle).[14] Combining interconnected and hollow nanostructures, Yao et al. prepared interconnected Si hollow NPs using solid SiO_2 spheres as template and demonstrated a quite impressive specific capacity and cycling stability of ≈1420 mAh g^{-1} after 700 cycles at 0.5 C discharge/charge rate.[15]

Here, we report a template-free and binder-free synthesis of high-rate and durable LIBs with a highly interconnected and hollow Si–Cu alloy (mixture) nanotube anode structure. A crossing matrix of CuO NW was first grown on copper foam (CF) substrate via a thermal oxidation in a furnace tube, as shown in **Figure 2**a,b. Then, a roughly conformal coating of a-Si:H layer over the CuO NWs was accomplished in a plasma-enhanced chemical vapor deposition (PECVD) system to produce a continuous a-Si:H shell layer that covers the whole surface complex and joins the crossing points of initially separated CuO NWs, as shown in the scanning electron microscopy (SEM) images in Figure 2c,d. After that, an in situ H_2 annealing at ≈450 °C was carried out to reduce the CuO cores into Cu, which then diffused into and alloyed with the a-Si:H shell to form a basically hollow and conductive nanotube (filled with discontinuous Cu segments inside), as shown in Figure 2d, inset. Taking this Si–Cu nanotube as self-sustainable anode structure, we have achieved a final specific capacity of ≈1010 mAh g^{-1} and ≈84% capacity retention after 1000 cycles at 3.4 A g^{-1}, or ≈780 mAh g^{-1} at 20 A g^{-1} with a high retention ratio of 88% for 1000 cycles without any binder or conductive agent. Surprisingly, this hollow Si–Cu alloy-nanotube-based LIB can even recover well (more than 90% capacity retention over 320 cycles) after 35 runs of extremely fast charging cycles at 70 A g^{-1}. These results indicate a whole new and promising routine to fulfill the true potential of high capacity Si-based LIB applications.

2. Results and Discussion

The fabrication process of the interconnected hollow Cu–Si alloy mixture nanotube anode structure has been schematically illustrated in Figure 1. First, the crossing CuO NWs were grown upon CF in a simple oxidation in air ambient at about 450 °C for 3 h, as shown in Figure 1a,b. Then, an a-Si coating shell was deposited in a PECVD with pure SiH_4 to cover the overall CuO NWs and merge the touching crossing joints of CuO NWs into continuous interconnected a-Si shell network that serves as an effective "binder," as illustrated in Figure 1c,d. Finally, to transform the CuO/a-Si core–shell structure into hollow tubular Cu–Si alloy mixture nanotubes, an H_2 atmosphere annealing

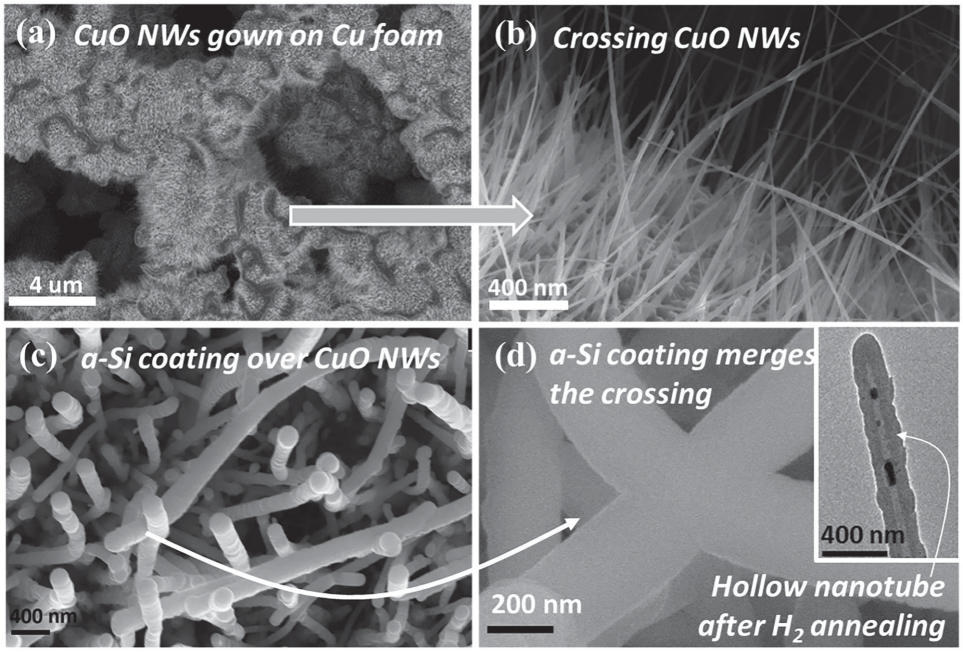

Figure 2. a,b) Low- and high-magnification SEM of crossing CuO NWs grown on copper foam, c) interconnected CuO/a-Si core–shell structure reduction at 450 °C for 4 h in H_2 atmosphere, and d) partial enlarged detail.

at around 450 °C was applied that reduces the CuO NW into Cu and diffuses into the a-Si shell to form self-sustainable and conductive Cu–Si nanotubes.

Figure 2a shows the typical SEM image of the as-prepared high density and crossing CuO NWs grown out of CF substrate in a simple atmosphere oxidation process. A close view of the tiny CuO NWs is provided in Figure 2b, showing a high density matrix of mutual crossing CuO NWs that measure around 2–3 µm long and 40–50 nm wide in the middle diameter. After a uniform coating of a-Si thin film upon the CuO NWs in PECVD system, as shown in Figure 2c, a CuO/a-Si core–shell structure is obtained with a diameter of around 300–350 nm, from which the sidewall coating thickness of the a-Si layer can be estimated to be around 130–150 nm. It is interesting to note that a relatively thick a-Si coating is also helpful to form interconnection, or in other words merge the CuO nanowires that are not touching initially, as shown in Figure 2d, to form a three-dimensional continuous a-Si shell network. And, the mutual crossing or connection among the a-Si-coated CuO NWs is indeed quite frequent, where a thick a-Si coating layer has played a critical role to bind them together to merge into a continuous 3D network as shown in Figure 2c,d. In addition, this a-Si coating shell could also enhance the mechanical attachment of the alloy nanotubes to the collector electrode underneath. After a reductive H_2 ambient annealing, the CuO cores can be effectively reduced into Cu, which then continues to diffuse and alloy with the a-Si shell. The Cu/a-Si core–shell nanotube structures, before or after H_2 ambient annealing under different temperatures, are also examined by XRD characterizations (where the whole structure with CF substrate are mounted upon the stage). According to the X-ray diffraction (XRD) analysis shown in **Figure 3**, a low-temperature H_2 annealing at 270 °C has been sufficient to activate the Cu–Si alloy forming process, leading to the emerging of several sharp diffraction peaks, located at 44.5° and 44.9° and correspond to the crystalline planes of Cu_3Si (012) and (300). At higher annealing temperature of 450 °C, the diffraction peaks of CuO all disappear indicating a thorough reduction and alloying of the core.

While the XRD analysis indicates a complete reduction of the CuO core and the alloy forming of Cu_3Si, it will be intriguing to examine the structural evolution or the spatial distribution of the newly formed Cu_3Si within the anneal core–shell structure. To this end, high-resolution transmission electron microscopy (HR-TEM) characterizations provide the most straightforward

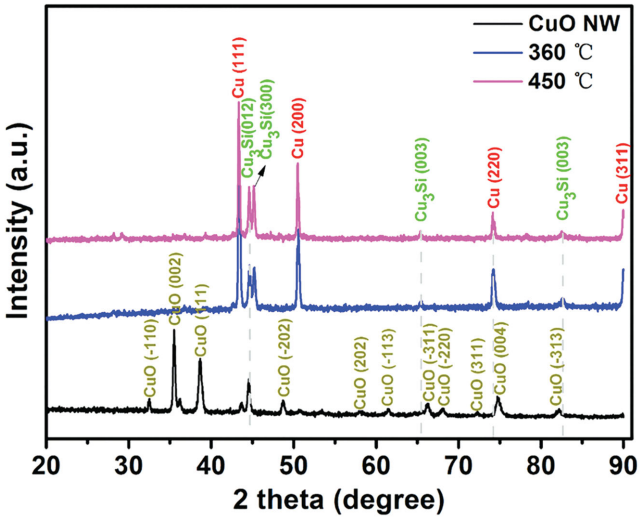

Figure 3. XRD analysis of CuO/a-Si core–shell NWs and CuO/a-Si core–shell reduced at 270, 360, and 450 °C for 4 h in H_2, respectively.

information. Though little morphology change can be observed for the samples before and after H_2 annealing, the CuO/a-Si core–shell structure experiences a dramatic mass migration inside leading to a basically hollow core region, as shown by a TEM imaging presented in the inset of Figure 2d. In more details, in the first row of **Figure 4**a–d, we show the dark field STEM image as well as the energy dispersive X-ray (EDX) mapping of Cu, Si, and O elements with a single CuO/a-Si core–shell NW after H_2 annealing at 270 °C for 4 h. It is clear that though the XRD analysis indicates a strong signal of alloy forming, the Cu core (or as a mixture of Cu and Cu_3Si) remains still at the center, with only a little amount of interdiffusion between the Cu core and a-Si shell. When the annealing temperature is raised to 450 °C, as shown in Figure 4e, the Cu core is observed to diffuse into the a-Si shell, forming a hollow nanotube structure with an alloy mixture of Cu–Si. Enlarged HR-TEM view into the Cu–Si alloy mixture shell, as shown in Figure 4f, reveals a high population of closely packed Cu_3Si NPs with a *d*-space of ≈0.20 nm corresponding to the (012) crystalline plane of Cu_3Si,[16] embedded within the a-Si shell matrix. Meanwhile, discontinuous Cu segments can also been found from place to place within the nanotubes, as shown in Figure 4e,g, where the *d*-space of 0.21 nm corresponds to the (111) plane of Cu.[17] These observations are indicating an interesting phenomenon that the Cu ingredient in the core can readily diffuse and migrate into the a-Si shell at an elevated annealing temperature of 450 °C, leading to the formation of a basically hollow tube inside which is highly beneficial to accommodating large volumetric expansion in Si lithiumization. In addition, as these Cu–Si alloy mixture nanotubes comprise a high density of Cu_3Si particle inclusion within the a-Si matrix, see Figure 4f for example, a largely enhanced conductivity in the shell storage layer can be expected.[16–19] This will make it possible to deposit a thicker a-Si medium layer (as more than 130 nm here compared to that <30 nm in ref. [12] to increase the overall mass loading of anode, which is also an important aspect for practical LIB applications.[12,13]

Figure 5a) shows the current–voltage curves of a LIB with highly interconnected Cu–Si alloy/mixture nanotube anode, where a large discharging current surge below 0.2 V can be assigned to the Li-ion insertions into the a-Si matrix and the crystallization process of a-$Li_{15}Si_4$.[13] In the reverse charging scan, the two oxidation current peaks at around 0.3 and 0.5 V correspond to the delithiation process of Li_xSi back to a-Si.[20–22] The voltage–capacity curves during the first five discharge/charge cycles are provided in Figure 5b. As we can see, while a relatively large extra discharging capacity has been observed in the first run, the following four cycles demonstrate basically identical charging and discharging curves. In the second cycle, lithium-ion insertion occurs at an earlier voltage stage of ≈700 mV, which has also been reported earlier and assigned to the surface formation of solid electrolyte interphase (SEI) film.[23,24] In addition, the highly interconnected Cu–Si nanotube anode shows an initial Coulombic efficiency of 42% with an irreversible first-run discharge capacity up to around 4000 mA g^{-1}, which can be attributed to an irreversible SEI film formation[23,24] and the chemical reaction between the Li ions and the background oxygen content in the CuO/a-Si core–shell matrix.[22,24,25] Meanwhile, it is also important to note that as the operation voltage window is set to from 0.01 to 1.1 V, lying far below the reaction voltage for Cu^{2+}/CuO reaction at 2.5 and 2.7 V, the Cu ingredient within the Cu–Si nanotubes will not participate or contribute to the lithium-ion storage in the following cycles.[22,26]

The cycling performances of the Cu–Si nanotube anodes at 0.84, 1.6, and 3.2 A g^{-1} during their initial 100 cycles are

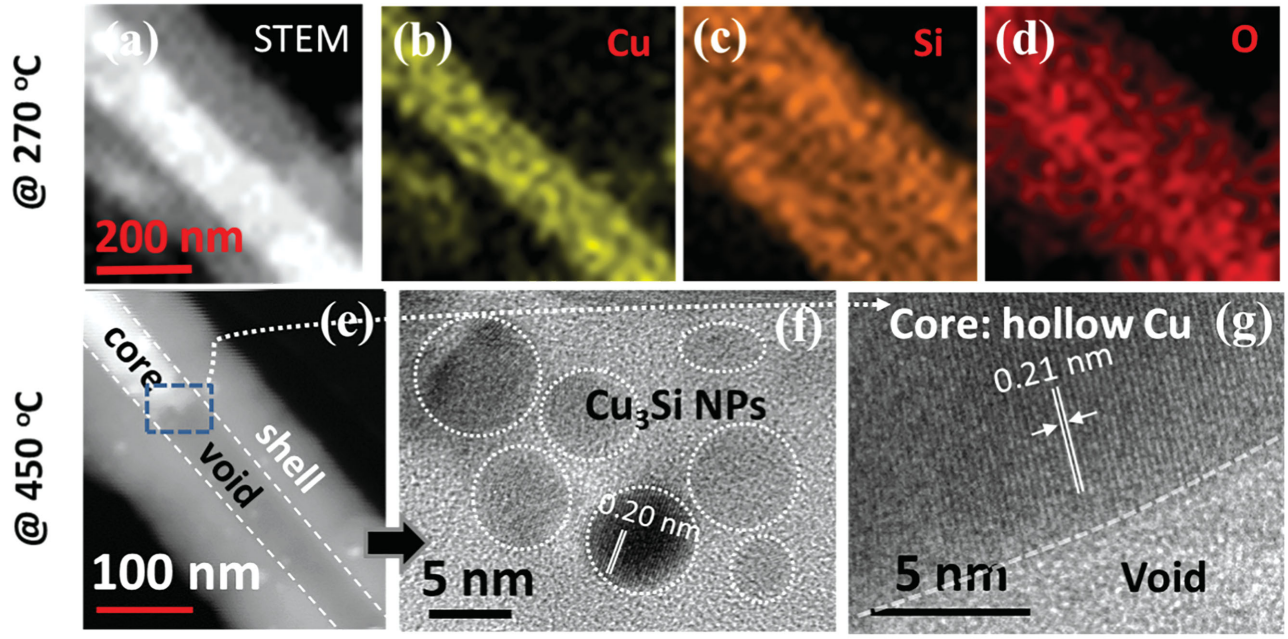

Figure 4. a–d) Annual dark-field STEM image and EDX mapping of CuO/a-Si (≈30 min) core shell including Cu, Si, and O element, e) STEM image of CuO/a-Si complex anode annealed in hydrogen atmosphere at 450 °C for 4 h, and f, g) high-resolution TEM image of amorphous silicon shell doped Cu_3Si NPs and hollow copper core.

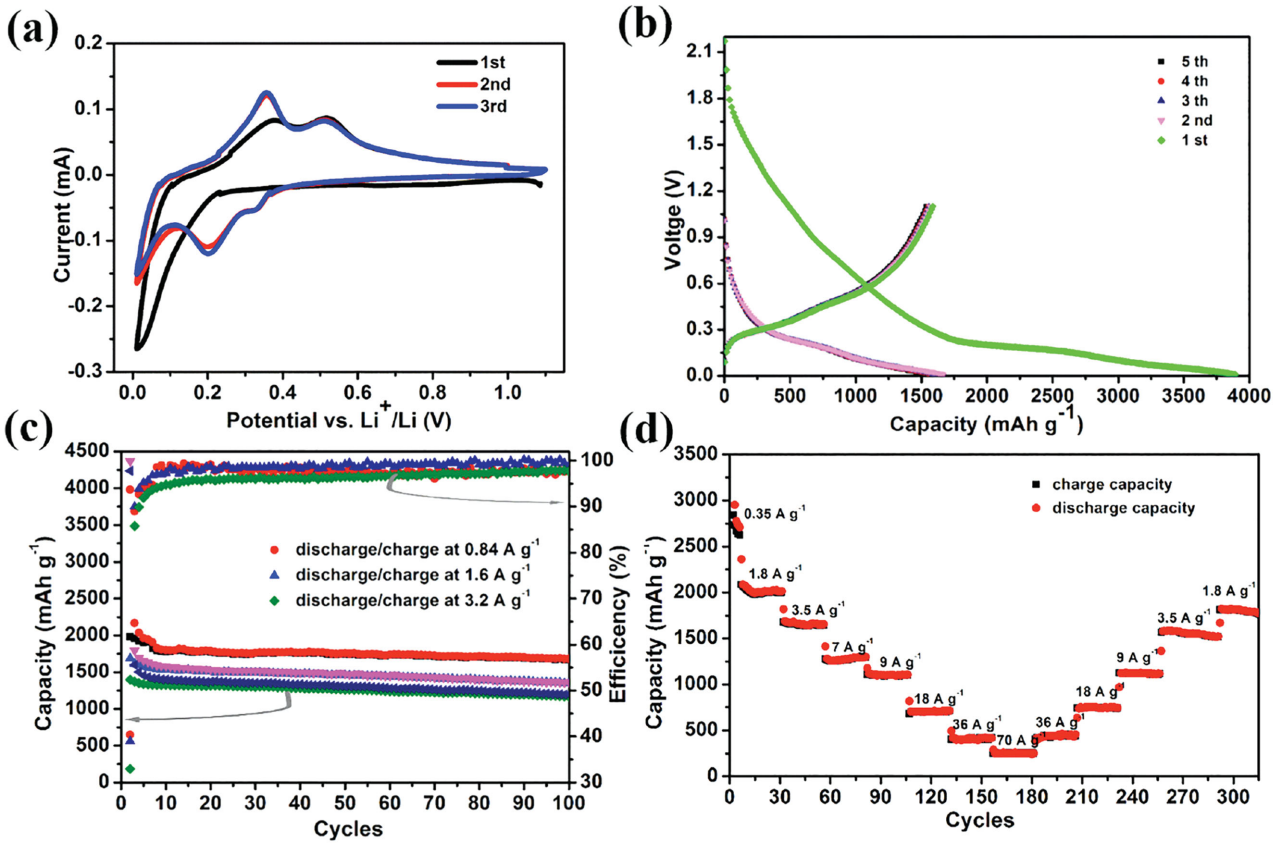

Figure 5. Li-ion battery cycling performance of highly connected hollow Cu–Si anode materials annealing in H_2 at 450 °C for 4 h between 0.01 and 1.1 V: a) cyclic voltammetry curves for the first three cycles of Cu–Si alloy mixture at a scan rate of 0.0001 V s^{-1} with the voltage range of 0.01–1.1 V, b) voltage profiles of the first five cycles at 1.6 A g^{-1}, c) the discharge capacities and corresponding Coulombic efficiencies of Cu–Si anode with the discharge/charge current of 0.84, 1.6, and 3.2 A g^{-1} over 100 cycles, respectively, and d) rate capability from 0.35 to 70 A g^{-1} discharge/charge current.

shown in Figure 5c, with corresponding specific capacities of 2160, 1790, and 1590 mAh g^{-1}, respectively. Their capacity retention rates are about 77.6%, 77.1%, and 76.2% from the 2nd to the 100th cycle, indicating a reasonably high specific capacity. Strikingly, as shown in Figure 5d, the Cu–Si nanotube anode demonstrates an excellent rate performance, with discharge capacities of about 1800, 1460, 1120, 970, 610, 360, and 220 mAh g^{-1} at discharge/charge current density of 1.8, 3.5, 7, 9, 18, and 70 A g^{-1}, respectively. More importantly, the specific capacity can be readily restored after experiencing a series of high-rate cycles up to 70 A g^{-1} (lasting 30 s at each current density step). The corresponding capacity retention ratios are ≈100% (≈360 mAh g^{-1}), ≈100% (≈610 mAh g^{-1}), ≈100% (≈970 mAh g^{-1}), ≈94% (≈1370 mAh g^{-1}), and ≈88% (≈1610 mAh g^{-1}) after 320 cycles. This outstanding high-rate performance and stability can be first attributed to the unique hollow Cu–Si nanotube anode structure with yet embedded Cu_3Si alloy NP inclusions that improve the electrical conductivity within the a-Si storage medium, which is a critical aspect to dissipate Li-ion insertion strain[19,20] during a high-rate charging and discharging operation. In addition, a hollow nanotube by itself is an advantageous geometry that will alleviate the volume expansion/contraction of the silicon medium during discharge/charge process.

Furthermore, these highly interconnected Cu–Si alloy anodes fabricated upon CF substrate also demonstrate an excellent long-term cycling performance compared to those grown on flat stainless steel (SS) where similar Cu–Si nanotubes are formed but rarely mutually crossing or connected (see the Supporting Information). **Figure 6**a shows the discharge/charge specific capacity evolutions of the Cu–Si nanotube anode samples fabricated upon CF or SS substrates at 3.4 A g^{-1} rate up to 1000 cycles. As we can see, though a relatively lower initial capacity is recorded for the CF nanotube sample, probably related to an incomplete reaction with the electrolyte in a complex and deep foam substrate, a final capacity as high as 1005 mAh g^{-1} can be obtained after 1000 cycles (corresponding to a 84% capacity retention). This compares largely advantageous to a much faster degradation of the capacity in isolated Cu–Si nanotube anodes fabricated on the SS substrate, where only a 400 mAh g^{-1} capacity (corresponding 24% capacity retention) can be retained. To testify the fast charging performance of this highly connected Cu–Si nanotube anode structure, we also carry out 1000 cycles of discharge/charge testing with a current density of 20 A g^{-1}. As shown in Figure 6b, a relatively high specific capacity of ≈780 mAh g^{-1} can be obtained, while an obvious activation process[24] is observed during the initial 80 cycles that increases the charge capacity from

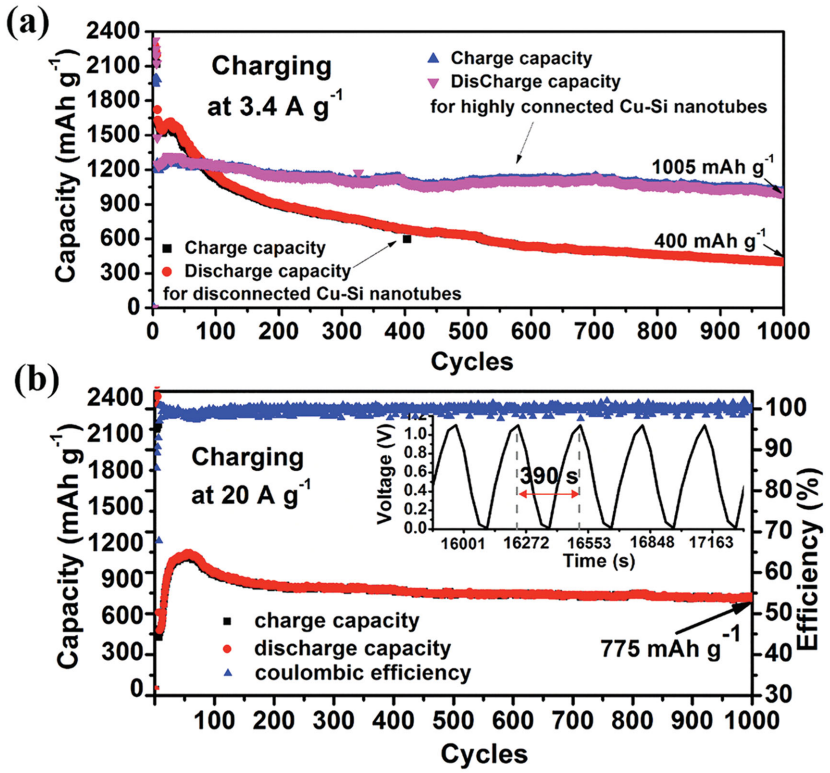

Figure 6. Li-ion battery cycling performance of Cu–Si anode materials between 0.01 and 1.1 V: a) long-term cycle performance of interconnected hollow Cu–Si nanotube anode and rarely connected hollow Cu–Si array reduction at 450 °C for 4 h at 3.4 A g^{-1} (≈30 min for one full discharge/charge process), and b) long-term cycle performance for Cu–Si anode reduction at 450 °C for 4 h at 20 A g^{-1} (≈3 min for one full discharge/charge process). Inset: charge and discharge cycles.

≈500 to 1100 mAh g^{-1}. Excluding the initial activation process, a retention rate is defined as the ratio of the final capacity to that obtained at the 200th cycle, to be ≈of 88%. This implicates indeed an ultrafast charging operation, as inferred from the inset in Figure 6b that allows a full battery charging process in ≈3 min with yet two times higher capacity than that of graphite LIBs (372 mAh g^{-1}).

Meanwhile, it is also important to emphasize that this interconnected Cu–Si nanotube structure provides a unique opportunity to achieve simultaneously a high-rate and durable anode material for LIBs to last 1000 cycles with a high capacity retention of >88%. In comparison to the available literature on similar core–shell structures, as summarized in **Table 1**, the stability issue (particularly under high-rate operation) still remains the most challenging one for promoting high-performance Si-loaded LIB applications. To guarantee the integrity of the Si storage medium, the Si coating layer has to be very thin, for example <30 nm in ref. [12] (and all the others below <100 nm in Table 1), to allow a fast extraction or insertion of Li ions into or out of the less conductive Si layer. Adopting a synergetic core–shell structure by itself would not be sufficient to address this issue. For instance, for a quite similar Cu/a-Si core–shell NW structure reported in ref. [27], without an alloy forming and migration that leading to a hollow nanotube structure, the cycling stability has been largely limited (up to 100 runs) though an excellent specific capacity and retention rate have been recorded. In contrast, in this work, the Cu ingredient has been activated to diffuse, migrate, and alloy into the a-Si shell, leaving a far more flexible hollow nanotube and conferring a high conductivity to the Si medium shell. In this way, a much thicker Si shell (≈130 nm) can be coated over the NW frameworks with achieving still an outstanding rate performance (charging/discharging at 70 A g^{-1}) and cycling stability (>1000 cycles), see the data in Figures 5 and 6. Therefore, combining an alloy-forming process to a highly connected 3D NW architecture (where multiple conductive paths ensure a durable operation) could indicate a whole new strategy to establish a robust, high-rate, and high storage density Si-based LIB.

3. Conclusions

In summary, we have proposed and fabricated here a new highly interconnected Cu–Si alloy mixture nanotube structure as anode in LIB. Without the use of any binder or conductive agent, the LIBs demonstrate a high capacity (≈2000 mAh g^{-1} at 0.84 A g^{-1}), high capacity retention performance of 84% (>88%) at 3.2 A g^{-1} (or 20 A g^{-1}) after 1000 cycles. In addition, this excellent anode material can withstand cycling at ≈70 A g^{-1} without damaging the rate performance of LIBs after 260 cycling. Such a highly interconnected hollow structure could also indicate an effective strategy to design high capacity alloy-type anode material systems for developing a high-performance and durable Si-based LIB application.

4. Experimental Section

Synthesis and Fabrication: Commercial CF from Suzhou Jiadelong with a thickness of 0.3 μm was used as a conductive substrate. The CF was first soaked in hydrochloric acid for 30 min and then dried under argon atmosphere. And, the crossing CuO NWs were grown upon CF by a simple oxidation in air ambient for 180 min at 450 °C in a conventional furnace tube. The vapor–solid (V) mechanism could be used to explain the growth of CuO NWs in the work.[35,36] Then, the sample was loaded into a PECVD system and CuO NW cores were coated with an a-Si shell layer by a glow discharge deposition of 5 sccm pure SiH_4 for 30 min at 200 °C, with an Si loading of about 0.18–0.21 mg cm^{-2}, a chamber pressure of 600 mTorr, and an RF power density of 76 mW cm^{-2}. Finally, the sample was annealed at 450 °C in H_2 for 240 min to reduce the CuO cores and transform the CuO/a-Si core–shell into hollow Cu–Si alloy mixture nanotubes with an H_2 flow rate and a chamber pressure of 45 sccm and 600 mTorr, respectively.

Characterizations and Test: The morphology, structure, and chemical composition of interconnected hollow Cu/a-Si core–shell were characterized by field emission SEM (FE-SEM, Sigma), TEM (Tecnai G2 F20), and EDX (Tecnai G2 F20). The electrochemical properties of the samples were measured in CR2032 coin-type cells assembled in an argon-filled glove box. The cells were formed using an Li metal negative electrode, an electrolyte of 1 M LiPF6 in a 1:1 ethylene

Table 1. A summary of the performances of different Si-loaded core–shell NW or nanotube structures from the 2nd to the last cycle in the literature,[10–13,27–34] in comparison to what is achieved in this work.

Materials and Structure	Thickness of Si shell [nm]	Current density [A g^{-1}]	Cycles	Capacity after cycles [mAh g^{-1}]	Capacity retention [%]	Reference
C @ Si @ C	≈20	0.3	60	≈2200	≈69	[33]
Nanotube array		0.2–0.84–0.2	50	≈1240	≈88	
Cu–Si core shell	≈50	0.84	400	≈1500	≈60	[28]
Nanotube array		1.3–50–1.3	50	≈410	≈97	
CNT-Si	≈12	2.0	50	≈980	≈57	[34]
Composite		2.0–3.0–2.0	30	≈1000	≈60	
Cu–Li_2O @ a-Si	≈40	0.84	100	≈2200	≈94	[22]
Core shell array		0.2–4.0–0.2	100	≈500	≈70	
Si nanotube	≈30	50	6000	≈600	≈88	[12]
		4.2–84–4.4	700	≈550	≈85	
Cu–Si–Al_2O_3	≈100	1.4	100	≈1560	≈90	[30]
Nanocable array		0.3–70–0.3	60	≈200	≈76	
Interconnected Si	–	8.4	72	≈1800	≈84	[13]
NW		0.4–34–0.4	70	≈420	≈84	
CNT-Si core shell	≈55	0.84	80	≈2510	≈91%	[31]
NW		0.84–50–0.84	77	≈980	≈94%	
CNT-Si NW	≈20	0.84	100	≈2500	≈91	[32]
		0.84–63	80	≈720	–	
Cu–$Si_{1-x}Ge_x$ core	≈60	4.0	75	≈1500	≈75	[29]
Shell NW array		0.63–10–0.63	40	≈1360	≈87	
Coaxial Cu–Si @	≈45	0.8	50	≈2400	≈82	[27]
C array		0.8–8.0	–	≈1050	–	
C-Si @ a-Si core shell NW array	≈47	3.4	100	≈880	99%	[10]
a-Si/carbon	≈60	0.84	55	≈1600	≈84	[11]
Nanofiber NW array		0.84–4.0–0.84	80	≈800	≈96	
Connected Cu–Si	≈120	3.4	1000	≈1000	≈84	This work
Alloy nanotube		20	1000	≈770	≈88	
		1.8–70–1.8	320	≈250	≈88	

carbonate and diethyl carbonate mixture. A galvanostatic cycling test of the assembled cells was carried out on a Land system (BT 2013A). Cyclic voltammetry characterizations were conducted with an electrochemical workstation (CHI660D) with a two-electrode system incorporating interconnected hollow Cu–Si alloy tubes as the working electrode and Li foil as the reference and counter electrodes. The mass load of a-Si was evaluated by a high-quality precision electronic balance (Sartorius, BT125D, 0.1 mg).

Supporting Information

Supporting information is available from Wiley Online Library or from the author.

Acknowledgements

H.S. and H.W. contributed equally to this work. This work was partly supported by Jiangsu Province Natural Science Foundation (Young Talent Program No. BK20130573), 333 Project of Jiangsu Province (BRA 2015284), National Basic Research 973 Program under Grant Nos. 2014CB921101, 2013CB932900, and 2013CB632101, NSFC under Grant Nos. 11274155 and 61204050, Scientific and Technological Support Programme in Jiangsu province under No. BE2014147-2, Jiangsu Shuangchuang Personal and Team's Program, and the Fundamental Research Funds for the Central Universities.

Received: September 21, 2015
Revised: October 26, 2015
Published online: December 15, 2015

[1] B. Kang, G. Ceder, *Nature* **2009**, *458*, 190.
[2] M. Armand, J.-M. Tarascon, *Nature* **2008**, *451*, 652.
[3] D. Larcher, J. M. Tarascon, *Nat. Chem.* **2015**, *7*, 19.
[4] C. K. Chan, H. Peng, G. Liu, K. McIlwrath, X. F. Zhang, R. A. Huggins, Y. Cui, *Nat. Nanotechnol.* **2008**, *3*, 31.
[5] R. A. Huggins, *J. Power Sources* **1999**, *81*, 13.
[6] Y. Sun, R. B. Sills, X. L. Hu, Z. W. Seh, X. Xiao, H. H. Xu, W. Luo, H. Y. Jin, Y. Xin, T. Q. Li, Z. L. Zhang, J. Zhou, W. Cai, Y. H. Huang, Y. Cui, *Nano Lett.* **2015**, *15*, 3899.

[7] H. Kim, Y. Son, C. Park, M. J. Lee, M. Hong, J. Kim, M. Lee, J. Cho, H. C. Choi, *Nano Lett.* **2015**, *15*, 4135.
[8] J. R. Szczech, S. Jin, *Energy Environ. Sci.* **2011**, *4*, 56.
[9] N. Liu, H. Wu, M. T. McDowell, Y. Yao, C. M. Wang, Y. Cui, *Nano Lett.* **2012**, *12*, 3315.
[10] L. F. Cui, R. Ruffo, C. K. Chan, H. L. Peng, Y. Cui, *Nano Lett.* **2008**, *9*, 491.
[11] L. F. Cui, Y. Yang, C. M. Hsu, Y. Cui, *Nano Lett.* **2009**, *9*, 3370.
[12] H. Wu, G. Chan, J. W. Choi, I. Ryu, Y. Yao, M. T. McDowell, S. W. Lee, A. Jackson, Y. Yang, L. B. Hu, Y. Cui, *Nat. Nanotechnol.* **2012**, *7*, 310.
[13] H. T. Nguyen, F. Yao, M. R. Zamfir, C. Biswas, K. P. So, Y. H. Lee, S. M. Kim, S. N. Cha, J. M. Kim, D. Pribat, *Adv. Energy Mater.* **2011**, *1*, 1154.
[14] Z. L. Zhang, Y. H. Wang, W. F. Ren, Q. Q. Tan, Y. F. Chen, H. Li, Z. Y. Zhong, F. B. Su, *Angew. Chem. Int. Ed.* **2014**, *53*, 5165.
[15] Y. Yao, M. T. McDowell, I. Ryu, H. Wu, N. Liu, L. B. Hu, W. D. Nix, Y. Cui, *Nano Lett.* **2011**, *11*, 2949.
[16] C. Y. Wen, F. Spaepen, *Philos. Mag.* **2007**, *87*, 5581.
[17] C. H. Chiu, C. W. Huang, J. Y. Chen, Y. T. Huang, J. C. Hu, L. T. Chen, C. L. Hsin, W. W. Wu, *Nanoscale* **2013**, *5*, 5086.
[18] J. Qi, Y. Masumoto, *Mater. Res. Bull.* **2001**, *36*, 1407.
[19] D. C. Johnson, J. M. Mosby, S. C. Riha, A. L. Prieto, *J. Mater. Chem.* **2010**, *20*, 1993.
[20] M. Y. Ge, J. P. Rong, X. Fang, C. W. Zhou, *Nano Lett.* **2012**, *12*, 2318.
[21] A. Esmanski, G. A. Ozin, *Adv. Funct. Mater.* **2009**, *19*, 1999.
[22] H. Wu, N. Du, H. Zhang, D. R. Yang, *J. Mater. Chem. A* **2014**, *2*, 20510.
[23] T. Song, J. L. Xia, J. H. Lee, D. H. Lee, M. S. Kwon, J. M. Choi, J. Wu, S. K. Doo, H. Chang,W. I. Park, D. S. Zang, H. Kim, Y. G. Huang, K. C. Hwang, J. A. Rogers, U. Paik, *Nano Lett.* **2010**, *10*, 1710.
[24] J. X. Wang, Q. B. Zhang, X. H. Li, B. Zhang, L. Q. Mai, K. L. Zhang, *Nano Energy* **2015**, *12*, 437.
[25] H. H. Li, X. L. Wu, H. Z. Sun, K. Wang, C. Y. Fan, L. L. Zhang, F. M. Yang, J. P. Zhang, *J. Phys. Chem. C* **2015**, *119*, 3495.
[26] D. W. Su, X. Xie, S. X. Dou, G. X. Wang, *Sci. Rep.* **2014**, *4*, 5753.
[27] H. Guan, X. Q. Wang, S. Chen, Y. Bando, D. Golberg, *Chem. Commun.* **2011**, *47*, 12098.
[28] L. M. Sun, X. H. Wang, R. A. Susantyoko, Q. Zhang, *J. Mater. Chem. A* **2014**, *2*, 15294.
[29] J. Z. Wang, N. Du, H. Zhang, J. X. Yu, D. R. Yang, *J. Power Sources* **2012**, *208*, 434.
[30] F. F. Cao, J. W. Deng, S. Xin, H. X. Ji, O. G. Schmidt, L. J. Wan, Y. G. Guo, *Adv. Mater.* **2011**, *23*, 4415.
[31] Y. Fan, Q. Zhang, C. X. Lu, Q. Z. Xiao, X. H. Wang, B. K. Tay, *Nanoscale* **2013**, *5*, 1503.
[32] Y. Fan, Q. Zhang, Q. Z. Xiao, X. H. Wang, K. Huang, *Carbon* **2013**, *59*, 264.
[33] J. Y. Liu, N. Li, M. D. Goodman, H. G. Zhang, E. S. Epstein, B. Huang, Z. Pan, J. Kim, J. H. Choi, X. J. Huang, J. H. Liu, K. J. Hsia, S. J. Dillon, P. V. Braun, *ACS Nano* **2015**, *9*, 1985.
[34] H. J. Lin, W. Weng, J. Ren, L. B. Qiu, Z. T. Zhang, P. N. Chen, X. L. Chen, J. Deng, Y. G. Wang, H. S. Peng, *Adv. Mater.* **2014**, *26*, 1217.
[35] X. C. Jiang, T. Herricks, Y. N. Xia, *Nano Lett.* **2002**, *2*, 12.
[36] M. Kaura, K. P. Muthe, S. K. Despande, S. Choudury, J. B. Singh, N. Verma, S. K. Gupta, J. V. Yakhmi, *J. Cryst. Growth* **2006**, *289*, 670.